Deconvolution Analyses of Differential Scanning Calorimetry Profiles of β-Crystallized Polypropylenes with Synchronized X-ray Measurements

Yuzo Yamamoto,[†] Yuichi Inoue,[†] Teruaki Onai,[†,‡] Chikashi Doshu,[†] Hiroshi Takahashi,[§] and Hiroki Uehara*,[||]

Department of Biological and Chemical Engineering, Gunma University, Kiryu, Gunma 376-8515, Japan, Department of Physics, Gunma University, Maebashi, Gunma 371-8510, Japan, and Department of Chemistry, Gunma University, Kiryu, Gunma 376-8515, Japan

Received December 5, 2006; Revised Manuscript Received January 29, 2007

ABSTRACT: Phase transformations during heating of β-crystallized isotactic polypropylenes were investigated by simultaneous SAXS, WAXD, and DSC measurements. The isotactic polypropylene samples containing the larger amount of β-form crystals were prepared by a temperature-gradient method or with the used of a nucleating agent. DSC deconvolution analysis successfully reproduced the duplicated endotherms and exotherms for both samples, considering WAXD and SAXS changes with heating. The obtained results indicated characteristic phase transformations during heating, including the temporary melting of the initial β-form and synchronized recrystallization into the α-form before the final melting of α-form crystals.

Introduction

Isotactic polypropylene (i-PP) produces different crystalline modifications (α-, β-, and γ-forms), depending on the crystallization conditions. The most stable of these modifications is the α-form, which is obtainable by the conventional melt-crystallization process. In contrast, the β-form is the metastable modification, which often appears for quenching from melt[1−3] and crystallization with temperature gradation[4−7] or specific nucleation agents.[8−15] Some reports[7,16−20] indicate that the β-form transforms into the α-form during heating, annealing, or drawing through the melt-recrystallization process. Zhou et al.[18] discussed the possibility of this crystalline transition from the β-form to the α-form, based on the wide-angle X-ray diffraction (WAXD) change during the heating of the series of the samples prepared with different amounts of nucleation agent. Asano et al.[21] also reported the simultaneous differential scanning calorimetry (DSC) and WAXD measurement results for an oriented β-form film. They claimed that three peaks on the DSC profile corresponded to the melting of the β-form, the crystallization into the α-form, and the final melting of the α-form.

Such duplicated DSC peaks are often observed for various polymers,[22−28] but their resolutions into each endotherm are seldom examined. In the case of ultrahigh molecular weight polyethylene, the fitting function composed by a combination of extreme and Lorenz functions was very effective for estimating the phase amounts of shish kebab morphologies.[25] Wang et al.[28] also determined the fraction of the γ-form for poly(propylene-*co*-ethylene) by applying peak resolution software, but the strict peak deconvolution is still difficult when both endotherm and exotherm are contained in the given profile. For analysis of such multiple dynamics correlating with each other, the simultaneous measurement of DSC and WAXD is preferred. Yoshida et al.[29−31] reported the characteristic melting behavior of the sample having polymorphism and crystallization behavior during DSC heating scan. Recently, X-ray measurements during these dynamic processes of i-PP have been successfully performed using a synchrotron radiation source.[10,32−35]

As mentioned above, the β-form of i-PP is obtainable through different routes. Corresponding crystalline orders of these β-forms reflect on their melting and recrystallization phenomena.[18] In this study, β-form crystals having different crystalline orders were prepared by a temperature-gradient method or with the use of a nucleating agent. Structural changes during heating were examined by simultaneous SAXS, WAXD, and DSC measurements using synchrotron radiation.

Experimental Section

Samples. Two different samples containing the β-form were investigated. One film sample was prepared by crystallization from the melted sample containing 0.1% β-nucleator of *N,N′*-dicyclohexyl-2,6-naphthalenedicarboxamide. The other trans-crystallized film sample was prepared by a temperature-gradient method, where the sample was crystallized while sandwiched between two hot plates kept at different temperatures (165 and 65 °C). For the trans-crystallized sample, the direction of the crystal growth was parallel to the normal of the film surface. The sample thickness was 150 μm for both cases.

Measurements. Simultaneous SAXS, WAXD, and DSC measurements were performed at Beamline 9C of the Photon Factory (PF) at the High-Energy Accelerator Research Organization (KEK), Tsukuba, Japan. The radiation X-ray beam from the PF ring operated at 2.5 GeV was monochromatized and focused by an optical system with a bent mirror and an Si(111) double-crystal monochromator. Further beam collimation was performed by means of three independent slit systems. The X-ray wavelength used was 0.15 nm. SAXS and WAXD data were collected simultaneously using two position sensitive proportional counters with an effective length of 100 mm (PSPC-10, Rigaku, Tokyo).[36] The sample-to-detector distances were 1000 mm for SAXS and 280 mm for WAXD. The detector for SAXS was set at the normal angle to the detecting face to be parallel with the incident beam direction. The detector for WAXD was set at the normal angle to the detecting

* Corresponding author. E-mail: uehara@chem.gunma-u.ac.jp.
[†] Department of Biological and Chemical Engineering, Gunma University.
[‡] Present address: Department of Physics, Gunma University, Maebashi, Gunma 371-8510, Japan.
[§] Department of Physics, Gunma University.
[||] Department of Chemistry, Gunma University.

10.1021/ma062784s CCC: $37.00
Published on Web 03/15/2007

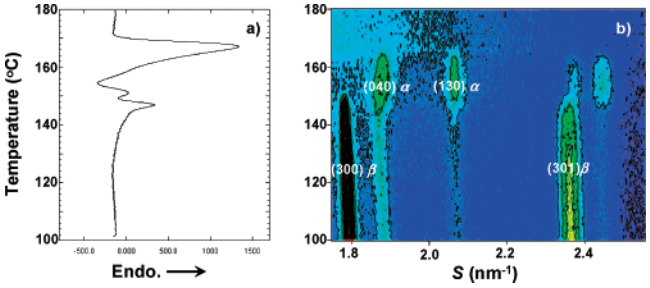

Figure 1. Simultaneous DSC (left) and WAXD (right) data during heating for the trans-crystallized sample. The WAXD profiles obtained at every 1 °C were duplicated with color gradation indicating intensity from lower blue to higher red. The typical (300) reflection of β-form crystals appears at $S = 1.80$ nm^{-1}. In contrast, (040) and (130) reflections of α-form crystals appear at $S = 1.87$ and 2.07 nm^{-1}. The heating rate was 2.0 °C/min.

face to have a tilt of 20° to the incident beam direction. The real spacing (d) and reciprocal spacing (S)

$$S = \frac{1}{d} = \frac{2 \sin \theta}{\lambda}$$

where 2θ is the scattering angle and λ is the wavelength of X-ray, were calibrated by diffraction patterns of powder crystals of silver behenate.[37] The sample temperatures were controlled using a FP84 differential scanning calorimeter (Mettler-Toledo K.K.), recording DSC signals simultaneously. The apparatus was set up for X-ray measurements according to Takahashi et al.[38] The temperature was calibrated by the melting point of indium and tin standards.

The film samples of PP were cut into square pieces with a size of ~4 × 4 mm^2. To ensure that the total thickness was 500 μm, three or four of the square PP pieces were accumulated and then wrapped in aluminum foil. The wrapped samples were fixed on the DSC apparatus, using an O-ring with a diameter of 4 mm.

Results and Discussions

First, the results of WAXD and DSC measurements were compared for the samples containing β-form prepared under different conditions. Figure 1 depicts the simultaneous WAXD and DSC data sets for the trans-crystallized sample. In WAXD results, both (300) and (301) reflections assigned to the β-form appeared before heating at room temperature with slight reflections of the α-form (040) and (130), the fraction of which corresponded to 20% in total reflection intensity.

The DSC thermogram exhibited multiple combinations of endothermic and exothermic peaks. The endotherm began from 130 °C, where the intensity reductions of both (300) and (301) reflections of the β-form were also recognized. Therefore, this endotherm could be ascribed to the melting of β-form crystals. At the nominal peak top at 147 °C, these β-form reflections almost disappeared. In contrast, the intensities of both (040) and (130) reflections of the α-form gradually increased with heating above 140 °C. Beyond the critical temperature of 147 °C, these α-form reflections became predominant. Further heating made them almost disappear at 167 °C, corresponding to the peak top of the main endotherm recorded on the DSC profile. These results indicated that this endotherm was attributed to the melting of α-form crystals. Another crystallization exotherm was sandwiched between these two melting endotherms of initial β-form and newly organized α-form crystals.

Similarly, the correlation between the DSC profile and the WAXD change during the same heating process was examined for the nucleation-crystallized sample (Figure 2). The DSC profile had a small exotherm at 142 °C, a subsequent small endotherm at 147 °C, and a final endotherm at 166 °C. The initial exothermic peak was characteristic for the nucleation-

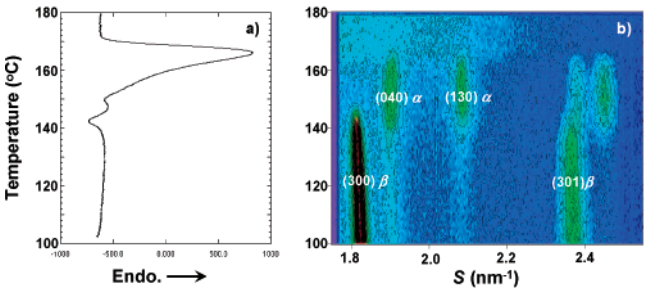

Figure 2. Simultaneous DSC (left) and WAXD (right) data during heating for the nucleation-crystallized sample. The heating rate was 2.0 °C/min. The representation of WAXD data is the same as in Figure 1.

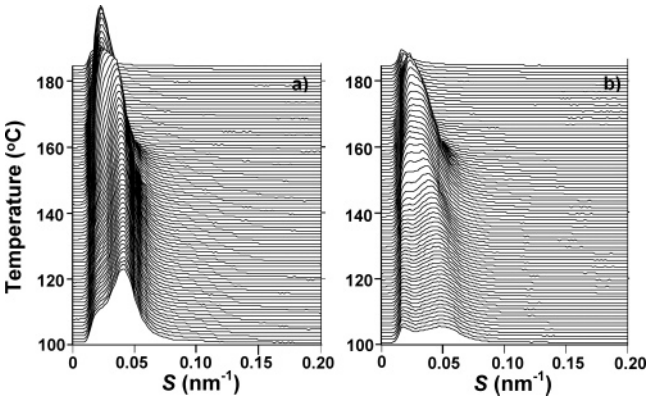

Figure 3. Simultaneous SAXS profiles recorded with WAXD and DSC data (Figures 1 and 2) during heating for the trans-crystallized (a) and nucleation-crystallized (b) samples. The heating rate was 2.0 °C/min.

crystallized sample, which was not observed for the trans-crystallized sample (see Figure 1). In the WAXD data, the intensities of (300) and (301) reflections of β-form began to decrease beyond 130 °C and completely disappeared at 145 °C. In contrast, the intensities of (040) and (130) reflections of α-form gradually increased with heating from 130 to 150 °C. These α-form reflections disappeared at 166 °C, which corresponded to the position of the final endotherm in the DSC profile. Thus, this final endotherm was attributed to the melting of α-form crystals. However, the decrease of the β-form and increase of the α-form overlapped in the temperature region containing the previous small exotherm and endotherm; therefore, the simple assignment of the DSC profile peaks was difficult. Their origins will be discussed later.

Figure 3 compares the series SAXS profiles simultaneously recorded with the above DSC and WAXD measurements during the same heating experiments for trans-crystallized and nucleation-crystallized samples. The lower S region below 0.015 nm^{-1} corresponded to the beam stopper, which provided the nominal shoulder at the nearest center for both samples. In the case of the trans-crystallized sample, the sharper peak appeared at $S = 0.04$ nm^{-1} even at 100 °C, where none of the DSC profile changed. Considering the WAXD results presented in Figure 1, the initial β-form crystals were composed of the lamellae having a long period of ~23 nm. It was reasonable that the initial morphology of the trans-crystallization provided ease of lamellar stacking across the film thickness. This SAXS peak gradually grew with heating at a similar S position, but rapidly decreased beyond 140 °C, where both decrease of β-form crystals and increase of α-form crystals overlapped in Figure 1, with the position shift of the scattering peak into the lower S side.

In contrast, the nucleation-crystallized sample exhibited broader scattering located at $S = 0.05$ nm^{-1}, corresponding to the smaller long period of 20 nm. The broad scattering meant lower periodicity of crystalline and amorphous arrangement; thus, the β-form crystals contained in the nucleation-crystallized sample did not exhibit typical lamellar morphology. It was thought that the characteristic crystallization induced from the nuclei would produce the anisotropic spherulite structure distributed with the sample. Beyond 130 °C, this broad scattering became sharper with the position shift into the lower S side, indicating the enhanced arrangement of crystalline and amorphous phases. Here, new scatterings nominally appeared at 140 °C at $S = 0.02$ nm^{-1} for both samples, but could be attributed to the shadow of the beam stopper.

We thought that these WAXD and SAXS changes could be correlated with the DSC profile shape. For the quantitative analyses of these data, the change in the integral intensity of each WAXD or SAXS peak was estimated. Here, the integral intensity means the sum of the corrected intensity values within the given S range. Background was subtracted before such summation analyses.

It should be noted that the nucleation-crystallized sample had a random chain and lamellar orientations, independent of the crystal transformation. However, the temperature gradient method for preparation of the trans-crystallized sample gave the parallel orientation of chains to the film surface and the perpendicular orientation of the lamellae (Supporting Information). Therefore, the observed intensities at the given S were corrected by the observed intensity $\times S$ for SAXS profiles of the trans-crystallized sample. In contrast, the observed intensity $\times S^2$ should be adopted in the random orientation for those of the nucleation-crystallized sample.

In the case of WAXD profiles, the series of the previous studies adopted uncorrected WAXD intensity for estimation of the component ratio of α- and β-forms in iPP samples.[1,11,15,19,20] In these references, the set of (300) reflection peak for β-form and (110) one for α-form was used as an index ratio of these forms. Unfortunately, our experimental setup using PSPC covers the S range lager than 1.7 nm^{-1}, which did not contain the position of (110) reflection of the α-form. Thus, we had to adopt the other reflections as the α-form index. However, the (040) reflection for the α-form alone is much weaker than the (300) one for the β-form, thus the outer (130) one was further summed for the accurate analysis of the index change of the α-form. Figures 4 and 5 display the integral intensity changes of the β-form (300) reflection and α-form (040) and (130) reflections during heating of the trans-crystallized and nucleation-crystallized samples. The differential curve was also calculated in terms of temperature for each crystalline form, which was represented in the vertical axis on the right side. The S range for integration of intensity for the (300) reflection of the β-form was 1.78−1.85 nm^{-1}. In contrast, that for the (040) and (130) reflections of the α-form was 1.86−1.93 nm^{-1}, which is not overlapped with the former (300) reflection of the β-form.

Considering that the DSC profile principally represented the quantitative change of the crystalline portion, such a differential curve could be compared to the DSC profile shape. Namely, the differential curve of the (300) reflection indicated the melting of β-form crystals, and that of the (040) and (130) reflections denoted the melting and recrystallization of α-form crystals. For the trans-crystallized sample depicted in Figure 4, the β-form intensity began to decrease beyond 130 °C and finally reached zero. In contrast, the α-form intensity began to increase beyond

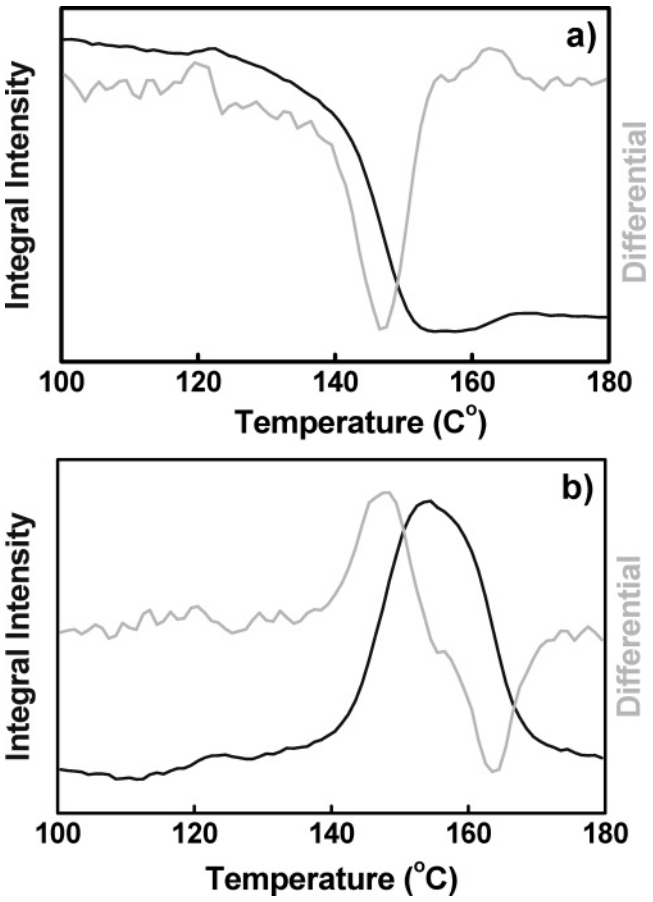

Figure 4. Changes in the WAXD integral intensities (thick lines) of the reflection peaks of the β-form (a) and the α-form (b) during heating for the trans-crystallized sample. The intensities of the (300) reflection peak with the S range from 1.78 to 1.85 nm^{-1} were integrated to represent the content of β-form crystals (a). Similarly, the α-form content was represented by the sum of the integral intensities of the (040) reflection S-ranging from 1.86 to 1.93 nm^{-1} and the (130) reflection S-ranging from 2.03 to 2.07 nm^{-1}. Their differential curves (gray lines) are also included.

140 °C and reached a maximum at 155 °C. Therefore, two peak tops were observed (148 and 164 °C), but at opposite sides for the differential curve. These peaks indicated the crystallization exotherm and melting endotherm of α-form crystals. These trends in the WAXD intensity changes with heating were kept even when the intensity correction was introduced (Supporting Information).

The nucleation-crystallized sample basically indicated a change similar to that of the trans-crystallized sample (Figure 5). The differences involved the positions of the peaks in the differential curves. The bottom side peak of β-form crystals appeared at 140 °C, which was lower than for the trans-crystallized sample. Correspondingly, the topside peak of the differential curve of α-form intensity appeared at 140 °C. These results suggested that the melting of β-form crystals necessarily followed the α-form crystallization. Namely, the α-form recrystallized from the melt provided by melting of the initial β-form crystals during the early stage of heating. In contrast, the bottom-side peak of the differential curve of α-form intensity was located at the same position as the trans-crystallized sample. This meant that melting erased the thermal history of the sample; thus, the final melting endotherm appeared at a constant temperature of 166 °C in the DSC profiles, independent of the initial morphology of the sample.

These reasonable correlations between WAXD and DSC results encouraged us to try the deconvolution analysis of DSC

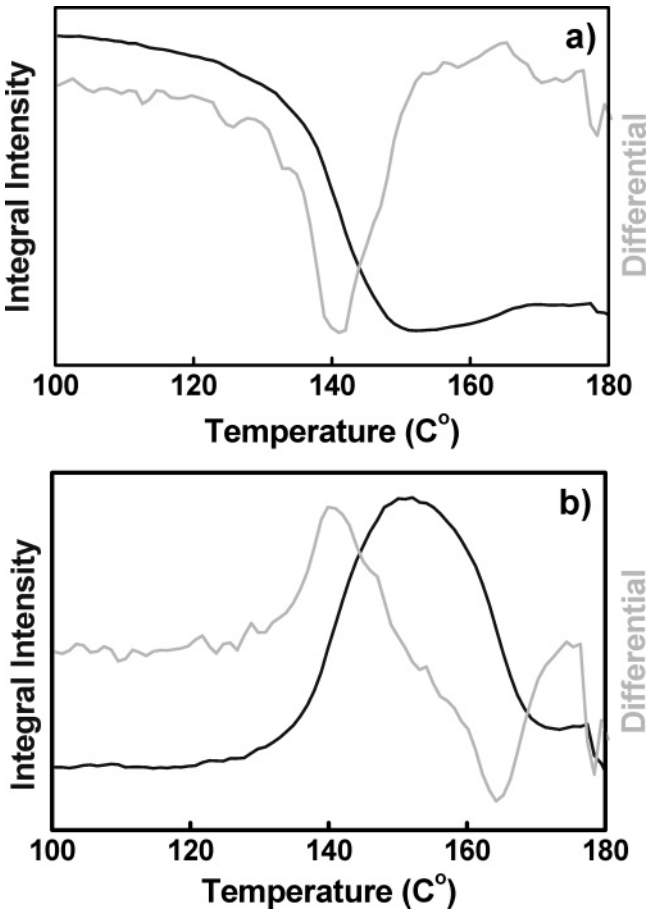

Figure 5. Changes in the WAXD integral intensities (thick lines) of the reflection peaks of the β-form (a) and the α-form (b) during heating for the nucleation-crystallized sample. The intensity estimations of both forms were the same (Figure 4). Their differential curves (gray lines) are also included.

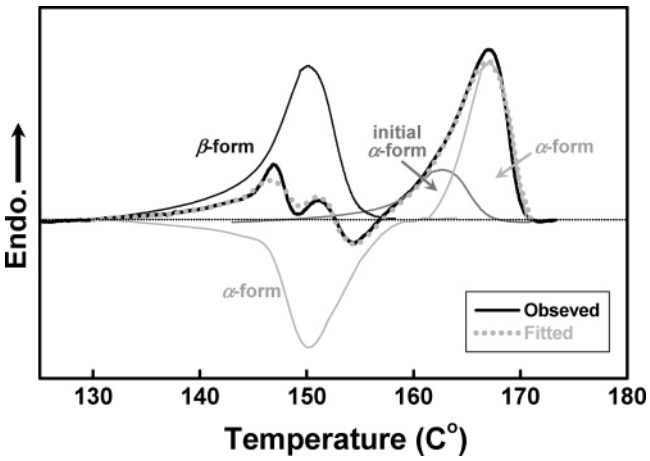

Figure 6. Deconvolution of DSC profile into the duplicated melting or crystallization contributions indicated by different lines for the trans-crystallized sample. The observed and fitted profiles are represented by solid and dotted lines.

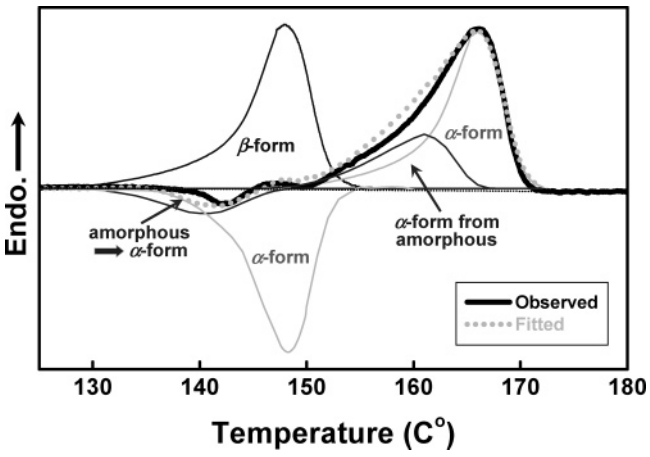

Figure 7. Deconvolution of DSC profile into the duplicated melting or crystallization contributions indicated by different lines for the nucleation-crystallized sample. The observed and fitted profiles are represented by solid and dotted lines.

profiles into the corresponding endotherms or exotherms. Commonly, the resolution of DSC profiles such as WAXD peaks has been difficult because the appropriate fitting function could not be adopted. However, it has been reported that the fitting function composed by a combination of extreme and Lorenz functions is successfully applicable for the DSC deconvolution analysis for polyethylene samples containing crystals having different melting temperatures.[25] One characteristic of this function is its asymmetrical set of slopes, which sandwich the endotherm top. The DSC peak of crystalline lamellae is necessarily composed by a combination of the gentle slope on the lower-temperature side and the steep slope on the higher-temperature side if the lamellae thickness distribution is unimodal, according to Thomson−Gibbs theory.[39] The peak position of each endotherm or exotherm could be estimated from the analytical results of the differential curves depicted in Figures 4 and 5. Thus, the unknown parameters could be simplified into peak height and width. Such reduction of the unknown parameters is very effective for appropriate fitting. Figure 6 reveals the fitting result for the DSC profile of the trans-crystallized sample. Considering the small but apparent amount of α-form crystals before heating (see Figure 1), the melting of such initial α-form crystals was further introduced. The melting of the β-form crystal began at 130 °C, with the peak top at 150 °C. Subsequent recrystallization into α-form crystals occurred in a similar temperature range. The melting of the initial α-form crystals was assigned to the shoulder peak located at 160 °C. The main endotherm also contained the final melting of the α-form crystals previously recrystallized at 150 °C. It should be noted that the multiple topside and bottom side peaks in the temperature range from 140 to 160 °C could be reproduced well in the resultant fitted profile.

For the nucleation-crystallized sample, the initial contents of the α-form crystals could be negligible (see Figure 2). However, the lower crystallinity of the initial morphology might require the additional cold-crystallization of the endotherm into α-form crystals. Considering the initial endotherm at 142 °C, such cold-crystallization was placed before the α-form crystallization from the melt provided by the initial β-form melting. Figure 7 compares the observed and fitted profiles. The melting of the cold-crystallized α-form crystals could be assigned as the shoulder peak located at 160 °C. Its peak position was comparable to that of melting of the initial α-form crystals for the trans-crystallized sample in Figure 6, but the origins of these peaks were different. A slight deviation between the observed and fitted profiles was recognized at 140 °C, but could be negligible in the other temperature range. Such coincidences of the observed and fitted curves described in these figures indicate that the total heat balance is nearly equal to zero for both samples.

Similar estimation of the integral intensity was also examined for the series of SAXS profiles depicted in Figure 3. The S range for such intensity integration was set from 0.02 to 0.10 nm^{-1} to include both the initial scattering peak and that newly formed

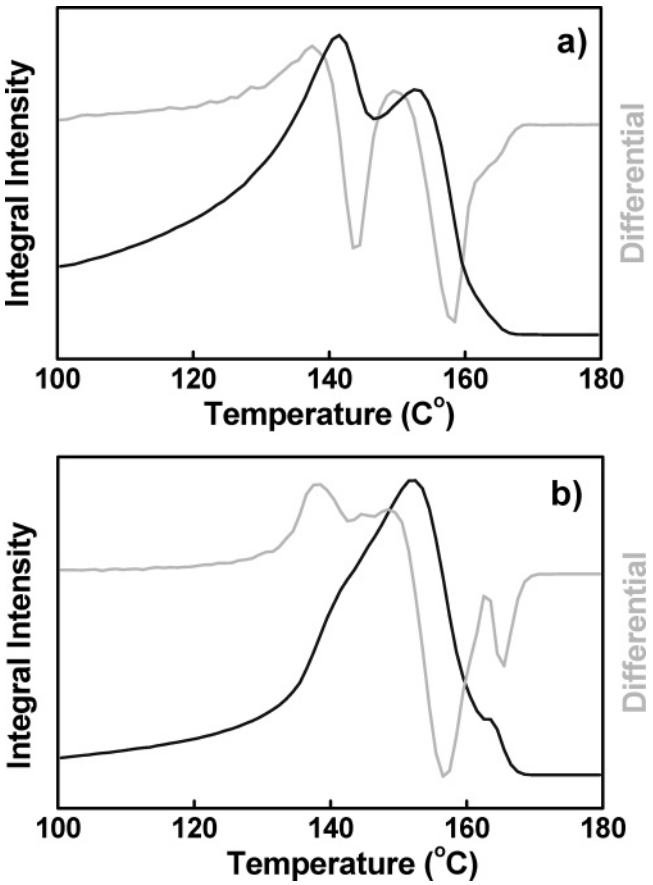

Figure 8. Changes in the SAXS integral intensity (thick lines) within the S range from 0.02 to 0.10 nm^{-1} during heating for the trans-crystallized (a) and nucleation-crystallized (b) samples. Their differential curves (gray lines) are also included. The intensity corrections by S and S^2 were introduced for the trans-crystallized and nucleation-crystallized samples.

during heating, but not the beam-stopper region below 0.015 nm^{-1}. The obtained results were compared (Figure 8) for the trans-crystallized and nucleation-crystallized samples with the corresponding differential curves. On the basis of the DSC fitting results in Figures 6 and 7, the origins of the peaks on the differential curves could be predicted. For the trans-crystallized sample, three bottom-side peaks (145, 157, and 166 °C) corresponded to the melting of β-form, initial, and newly formed α-form crystals. The positions of the former two peaks deviated slightly from those indicated by DSC deconvolution analysis. This phenomenon could be ascribed to the overlapping of the topside peaks between them, which originated from crystallization of α-form crystals. In other words, the melt obtained from initial β-form crystals could be crystallized into the lamellar morphology during heating. This result of the integral intensity change was co-incident to the fact that the new scattering peak appeared beyond 145 °C (Figure 3).

In contrast, the nucleation-crystallized sample exhibited the characteristic topside peak at 140 °C in the differential curve. This exothermic peak was assigned to cold-crystallization into α-form crystals due to the lower crystallinity of this sample. In contrast, the melting peak of the β-form crystals was not detectable, indicating a nonlamellar morphology of the nucleation-crystallized sample. This agreed well with the broader scattering peak shape for this sample (Figure 3). However, the melting peak of the newly formed α-form crystals was observed at the same temperature for the trans-crystallized sample, which was also revealed by the DSC deconvolution result depicted in Figure 7. These analytical coincidences suggested that simultaneous WAXD, SAXS, and DSC measurements are very effective for tracing the complicated structural change of our β-crystallized i-PP samples even having different morphologies.

The transformation from the oriented lamellar stacking for initial β-form crystals to the non-oriented spherulite morphology for the recrystallized α-form crystals could affect the trend of the X-ray intensity changes for the trans-crystallized sample. Therefore, we tried the additional SAXS analysis without considering the effect of chain or lamellar orientation, i.e., using the intensity corrected by S^2, as same as the nucleation-crystallized sample (Supporting Information). The obtained results exhibited the similar trends in the differential curve for SAXS data. This means that the changes in the chain or lamellar orientation with melting/recrystallization are less pronounced on the analytical methodology adopted in this study, when the one-dimensional PSPS detector was applied. Future two-dimensional analysis of X-ray data may give us the information on the lamellar and chain orientation changes during heating of the series of β-crystallized iPP samples.

Conclusions

In this study, the β-form of i-PP could be prepared by a trans-crystallization procedure performed by a temperature-gradient method or by cooling crystallization with a nucleating agent of *N,N′*-dicyclohexyl-2,6-naphthalenedicarboxamide. Simultaneous DSC and WAXD measurements of these β-crystallized i-PP samples revealed that melting of the β-form was followed by crystallization into the α-form. DSC profiles of these samples looks quite different, but detailed analysis by DSC deconvolution procedure revealed similar phase transformations during heating: (1) the β-form temporarily melts, (2) the molten amorphous mass crystallizes into the α-form, and (3) this α-form finally melts. Synchronized SAXS measurements clarified that these β-crystallized i-PPs have different morphologies, depending on the thermal histories of the samples.

Acknowledgment. Simultaneous WAXD, SAXS, and DSC measurements were performed under approval of the Photon Factory Program Advisory Committee (Proposal 2004G265). This work was partly supported by Industrial Technology Research Grant Program in '04 from the New Energy and Industrial Technology Development Organization (NEDO) of Japan.

Supporting Information Available: Text discussing the orientation of trans-crystallized sample, effect of intensity correlation for WAXD profiles, and effect of lamellar orientation change for SAXS analyses and figures showing WAXD and SAXS patterns for the trans-crystallized sample recorded with the incident X-ray beam parallel to the film surface, changes in the WAXD integral intensities and their differential curves during heating, and changes in the SAXS integral intensity and its differential curve during heating. This material is available free of charge via the Internet at http://pubs.acs.org.

References and Notes

(1) Tuner, Jones, A.; Aizlewood, J. M.; Beckett, D. R. *Makromol. Chem.* **1964**, *75*, 134.
(2) Samuels, R. J.; Yee, R. Y. *J. Polym. Sci., Part A2* **1972**, *10*, 385.
(3) Padden, F. J.; Keith, H. D. *J. Appl. Phys.* **1959**, *30*, 1479.
(4) Fujiwara, Y. *Colloid Polym. Sci.* **1975**, *253*, 273.
(5) Lovinger, A. J.; Chua, J. O.; Gryte, C. C. *J. Polym. Sci., Polym. Phys. Ed.* **1977**, *15*, 641.
(6) Asano, T.; Fujiwara, Y. *Polymer* **1983**, *24*, 925.
(7) Yamamoto, Y.; Nakazato, M.; Saito, Y. *Netsu Sokutei* **1989**, *16*, 58.
(8) Li, J. X.; Cheung, W. L.; Chan, C. M. *Polymer* **1999**, *40*, 2089.
(9) Broda, J. *J. Appl. Polym. Sci.* **2004**, *91*, 1413.
(10) Chu. F.; Yamaoka, T.; Kimura, Y. *Polymer* **1995**, *36*, 2523.

(11) Fujiyama, M.; Kawamura, Y.; Wakino, T.; Okamoto, T. *J. Appl. Polym. Sci.* **1988**, *36*, 985.
(12) Varga, J. *J. Therm. Anal.***1989**, *35*, 1891.
(13) Fillon, B.; Thierry, A.; Wittmann, J. C.; Lotz, B. *J. Polym. Sci., Polym. Phys. Ed.***1993**, *31*, 1407.
(14) Shi, G.; Zhang, X.; Cao, Y.; Hong, J. *Makromol. Chem.* **1993**, *194*, 269.
(15) Cho, K.; Saheb, D. N.; Choi, J.; Yang, H. *Polymer* **2002**, *43*, 1407.
(16) Marigo. A.; Marega, C.; Causin, V.; Ferrart, P. *J. Appl. Polym. Sci.* **2004**, *91*, 1008.
(17) Verga, J.; Toth, F. *Makromol. Chem. Makromol. Symp.* **1986**, *5*, 213.
(18) Zhou, G.; He, Z.; Yu, J.; Han, Y.; Shi, G. *Makromol. Chem.* **1986**, *187*, 633.
(19) Marigo, A.; Marega, V.; Causin, V.; Ferrai, P. *J. Appl. Polym. Sci.* **2004**, *91*, 1008.
(20) Yuan, Q.; Jiang, W.; An, L. *Colloid Polym. Sci.* **2004**, *282*, 1236.
(21) Asano, T.; Yamamoto, T.; Mina, M. F.; Fujuwara, Y.; Takahashi, H.; Hatta, I. *J. Macromol. Sci. Phys.* **1999**, *B38*, 163.
(22) Harasawa, J.; Uehara, H.; Yamanobe, K.; Komoto, T.; Terano. M. *J. Mol. Struct.* **2002**, *610*, 133.
(23) Uehara, H.; Yamazaki, Y.; Ohotake, T.; Kanamoto, T. *Kobunshi-Ronbunshu* **1994**, *51*, 597.
(24) Nakae, M.; Uehara, H.; Kanamoto, T.; Ohama, T.; Porter, R. S. *J. Polym. Sci., Polym. Phys. Ed.* **1999**, *37*, 1921.
(25) Nakae, M.; Uehara, H.; Kanamoto, T. *Macromolecules* **2000**, *33*, 2632.
(26) Matsuda, T.; Aoike, T.; Uehara, H.; Yamanobe, T.; Komoto, T. *Polymer* **2001**, *42*, 5013.
(27) Aoike, T.; Yokoyama, D.; Uehara, H.; Yamanobe, T.; Komoto, T. *Wear* **2007**, *262*, 742.
(28) Wang, S.; Yang, D. *J. Polym. Sci., Polym. Phys. Ed.* **2004**, *42*, 4320.
(29) Yoshida, H.; Kinoshita, R.; Teramoto, Y. *Thermochim. Acta* **1995**, *264*, 173.
(30) Yoshida, H. *Thermochim. Acta* **1995**, *267*, 239.
(31) Yoshii, T.; Yoshida, H.; Kawai, T. *Thermochim. Acta* **2005**, *431*, 177.
(32) Iijima, M.; Strobl, G. *Macromolecules* **2000**, *33*, 5204.
(33) Somani, R. H.; Hsiao, B. S.; Nogales, A.; Srinivas, S.; Tsou, A. H.; Sics, I.; Balta-Calleja, F. J.; Ezquerra, T. A. *Macromolecules* **2000**, *33*, 9385.
(34) Assouline, E.; Grigull, S.; Marom, G.; Wachtel, E.; Wagner, H. D. *J. Polym. Sci., Polym. Phys. Ed.* **2001**, *39*, 2016.
(35) Nogales, A.; Hsiao, B. S.; Somani, R. H.; Srinivas, S.; Tsou, A. H.; Balta-Calleja, F. J.; Ezquerra, T. A. *Polymer* **2001**, *42*, 5247.
(36) Abe, S.; Takahashi, H. *J. Appl. Crystallogr.* **2003**, *36*, 515.
(37) Blanton, T. N.; Huang, T. C.; Toraya, H.; Hubbard, C. R.; Robie, S. B.; Louer, D.; Gobel, H. E.; Will, G.; Gilles, R.; Raftery, T. *Powder Diffr.* **1995**, *10*, 91.
(38) Takahashi, H.; Matuoka, S.; Amemiya, Y.; Hatta, I. *Chem. Phys. Lipids* **1995**, *76*, 115.
(39) Matsuda, T.; Aoike, T.; Uehara, H.; Yamanobe, T.; Komoto, T. *Kobunshi-Ronbunshu* **2001**, *58*, 326.

MA062784S